Article

Engineering Zeolitic-Imidazolate-Framework-Derived Mo-Doped Cobalt Phosphide for Efficient OER Catalysts

Mohammad Atiqur Rahman, Ze Cai, Zannatul Mumtarin Moushumy, Ryuta Tagawa, Yoshiharu Hidaka, Chiyu Nakano, Md. Saidul Islam, Yoshihiro Sekine, Yuta Nishina, Shintaro Ida, and Shinya Hayami*

Read Online

ACCESS | Metrics & More | Article Recommendations | SI Supporting Information

ABSTRACT: Designing a cheap, competent, and durable catalyst for the oxygen evolution reaction (OER) is exceedingly necessary for generating oxygen through a water-splitting reaction. In this project, we have designed a ZIF-67-originated molybdenum-doped cobalt phosphide (CoP) using a simplistic dissolution−regrowth method using Na_2MoO_4 and a subsequent phosphidation process. This leads to the formation of an exceptional hollow nanocage morphology that is useful for enhanced catalytic activity. Metal−organic frameworks, especially ZIF-67, can be used both as a template and as a metal (cobalt) precursor. Molybdenum-doped CoP was fabricated through a two-step synthesis process, and the fabricated Mo-doped CoP showed excellent catalytic activity during the OER with a lower value of overpotential. Furthermore, the effect of the Mo amount on the catalytic activity has been explored. The best catalyst (CoMoP-2) showed an onset potential of around 1.49 V at 10 mA cm^{-2} to give rise to a Tafel slope of 62.1 mV dec^{-1}. The improved catalytic activity can be attributed to the increased porosity and surface area of the resultant catalyst.
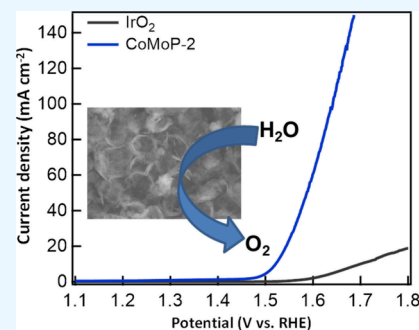
INTRODUCTION

The burgeoning industrial society and its rapid population growth have made energy scarcity and environmental issues paramount concerns for humankind. As a result, scientists have become dedicated to creating energy storage technologies that are both ecologically benign and effective. For future energy supply, it is critically necessary to develop low-cost, environmentally friendly, and highly efficient energy sources.[1] In this concern, electrochemical water splitting, which consists of both the hydrogen evolution reaction (HER) and the oxygen evolution reaction (OER) is particularly effective. The efficiency of each of these two processes can be boosted by accelerating the activity of the catalysts used in the cathode and anode while reducing the overpotential of the corresponding electrode.[2] Currently, noble metals such as IrO_2, RuO_2, and their amalgamations are considered as the most efficient catalysts for the OER. Unfortunately, high cost, low abundance, sluggish reaction kinetics, and low durability have narrowed the widespread use of these catalysts for practical applications.[3−6] Consequently, researchers are focused on the replacement of these noble-metal-based catalysts with earth-abundant electrocatalytically active materials. The catalysts' porous nanostructure would be a crucial step in exposing the active sites to the electrolyte and substrate as much as possible in order to attain high catalytic activity. Metal−organic frameworks (MOFs) are a class of porous crystal materials with ordered structures that seem like perfect antecedents in this situation. They provide an excellent surface area, distinct porosity, and adaptable activity. Even though a wide variety of

MOFs have been created to catalyze the oxygen release reaction, the majority of MOFs are unstable and are therefore unsuitable for most practical uses. On the other hand, metal Zeolitic imidazolate frameworks (ZIFs) (the skeleton of which consists of Co^{2+} ions coordinated with the N atoms of 2-methylimidazole and build a tetrahedral structural units) are highly promising because they offer several scientific and technological prospects, such as unique structure, easy fabrication, high surface area, tunable porosity, and high thermal and chemical stability.[7,8] Additionally, their structure and morphology can be tuned to get the desired structure and morphology with enhanced activity for application in energy devices. For instance, direct calcination of ZIF-67 results in the formation of a Co@N-doped carbon composite which showed enhanced catalytic activity toward the oxygen reduction reaction (ORR).[9] Moreover, ZIF can be renovated into various Co-containing catalysts, such as CoP, CoS, Co_3O_4, Co_3S_4, Co_9S_8, etc.,[10−15] that exhibit enhanced HER, OER, and ORR activity. Among them, researchers were focused on transition metal phosphides for application as overall water splitting catalysts, which include CoP, MoP, Ni_2P, and FeP. Unfortunately, the observed catalytic activity of these materials

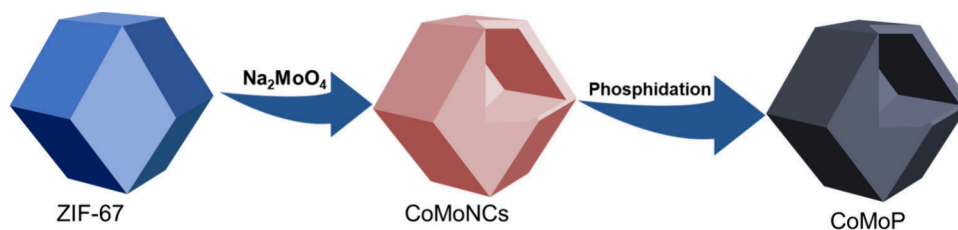**Scheme 1. Schematic Illustration of the Formation of ZIF-67-Derived Hollow CoMoP Nanocages**

is far behind the noble-metal-based catalysts. Additionally, complicated synthetic methods and sophisticated fabrication methods further restrict their practical applications.[32] Among the metal phosphide catalysts, cobalt phosphides attract interest because of their enhanced catalytic activity and morphologies such as nanorods, nanowires, nanoparticles, and nanosheets as well as ternary phosphides.[34,38] However, in order to obtain very durable electrocatalysts, unencapsulated Co nanoparticles within N-doped carbon cages have to be removed by an acid-washing phase, which raises production costs and lowers the amount of active species. Furthermore, efficient utilization of the active species is challenging because the agglomeration of the active components that occurs during the thermal treatment provides additional challenges in the development of a high-performance and durable MOF-based catalyst.[16−19] Recently, ZIF-67-derived hollow nanocages have attracted significant attention due to exciting structural and morphological characteristics such as high electrochemical active sites, low density, high porosity, and robust surface area. Although recent strategies for the synthesis of MOF-derived hollow nanocages utilize both hard and soft templates, these suffer from complex synthetic steps and removal processes. Interestingly, MOFs can be utilized both as precursors and templates for the synthesis of hollow nanocages with interesting structures and morphologies.[20−22] Recently some researchers explored the potential of doped and undoped nanocages as electrodes for a supercapacitor with enhanced performance and stability for practical applications.[24] Inspired by the above discussion, we have fabricated a ZIF-67-derived Mo-doped cobalt phosphide hollow nanocage (CoMoP) using a simple dissolution−regrowth method using Na_2MoO_4, which formed $CoMoO_4−Co(OH)_2$ hollow nanocages, and a subsequent phosphidation process (Scheme 1).

In our present work, we have fabricated Mo-doped CoP catalysts for application as catalysts for oxygen evolution reactions. This doping strategy improves the catalytic performance of the cobalt active site toward the OER. We have also analyzed the effect of the amount of Mo-dopant on the efficiency of catalytic activity, which was not reported yet. Especially, the hollow nanostructure with feasible nanostructure has interesting physical and chemical properties such as rich electrochemical active sites, low density, high surface area, and easy ionic accessibility, which makes them useful for electrochemical application. Additionally, easy fabrication and a self-sacrificed templating strategy allow for structural engineering for specific applications. The exceptional hollow morphology and synergistic interaction of both cobalt and molybdenum give rise to outstanding catalytic activity in terms of low overpotential, high current density, and considerable durability. The electrochemical measurements confirm that the as synthesized CoMoP displays notable electrocatalytic activity toward the oxygen evolution reaction (OER) under alkaline condition.

■ EXPERIMENTAL SECTION

Analytical grade chemicals were utilized prior to any kind of refinement.

Synthesis of ZIF-67. ZIF-67 was prepared using the method described in the literature.[23] Typically, cobalt nitrate ($Co(NO_3)_2·6H_2O$, 1.436 g) and 2-methylimidazole (3.244 g) were each dissolved in 100 mL of methanol. Subsequently, the solution containing metal salt was added into the ligand solution while stirring vigorously. Subsequently, the mixture was stirred for an additional 30 min and then kept undisturbed for 24 h. Finally, ZIF-67 was collected through centrifugation and purified using methanol 3 times and dried under vacuum at 60 °C for 12 h.

Synthesis of $CoMoO_4−Co(OH)_2$ Nanocages (Co-MoNCs). $CoMoO_4−Co(OH)_2$ nanocages were synthesized from ZIF-67 using the method described in the literature with some modification.[24] At first, 150 mg of ZIF-67 was dispersed in 50 mL of ethanol under sonication and vigorous stirring for 1 h. Then, a solution containing different amounts of $Na_2MoO_4·2H_2O$ dissolved in water was quickly added into the above solution. This mixture was refluxed for 3 h. Finally, the sample was collected after washing several times using water and ethanol. The dried sample was obtained after being freeze-dried for 2 days. Three different ratios of ZIF-67 to $Na_2MoO_4·2H_2O$ were used and named as CoMoNCs-1 (2:1), CoMoNCs-2 (1:2), and CoMoNCs-3 (1:3).

Fabrication of Mo-Doped CoP. The as-synthesized ZIF-67 or CoMoNCs and $NaH_2PO_2·2H_2O$ were placed at two different locations in a porcelain boat and inserted into a tube furnace while positioning $NaH_2PO_2·2H_2O$ at the upstream side of the furnace. The furnace was allowed to heat at 350 °C for 2 h with temperature rise of 2 °C per minute. The impurities and unstable compositions were washed away using 2 M HCl and washing with deionized water to get sample CoP, CoMoP-1, CoMoP-2, and CoMoP-3 while using sample ZIF-67, CoMoNCs-1, CoMoNCs-2, and CoMoNCs-3, respectively.

Evaluation of Catalytic Activity. Catalytic activity was investigated under ambient conditions using a three-electrode system fitted with a rotating (ring) disk electrode and potentiostat (RRDE-3A). Five milligrams of the sample was at first dispersed in 950 μL of ethanol using ultrasonication which was followed by the addition of 50 μL of Nafion solution (0.5 wt %). Then 5 μL of the sample was loaded on the working electrode (GCE, 3 mm in diameter) and dried at room temperature before starting the electrochemical measurement. All of the prepared catalysts were loaded on the surface of a glassy carbon electrode by simple drop casting with a loading of 0.35 mg cm^{-2}. All of the electrochemical measurements were performed using a Ag/AgCl electrode as the reference electrode and a graphite electrode as the counter electrode. All of these measurements were performed in 1.0 M
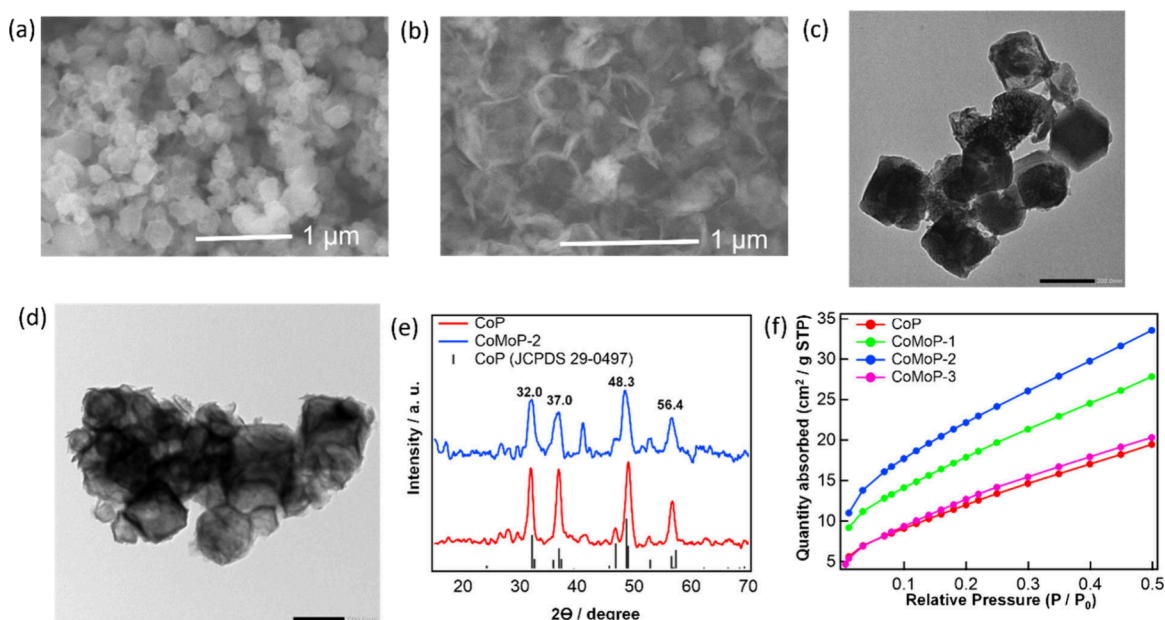
Figure 1. Surface morphology and characterization of the synthesized catalysts: SEM image of (a) CoP and (b) CoMoP-2; TEM images of (c) CoP and (d) CoMoP-2; (e) PXRD pattern of CoP and CoMoP-2; and (f) N_2 adsorption isotherm of CoP and Mo-doped CoP.
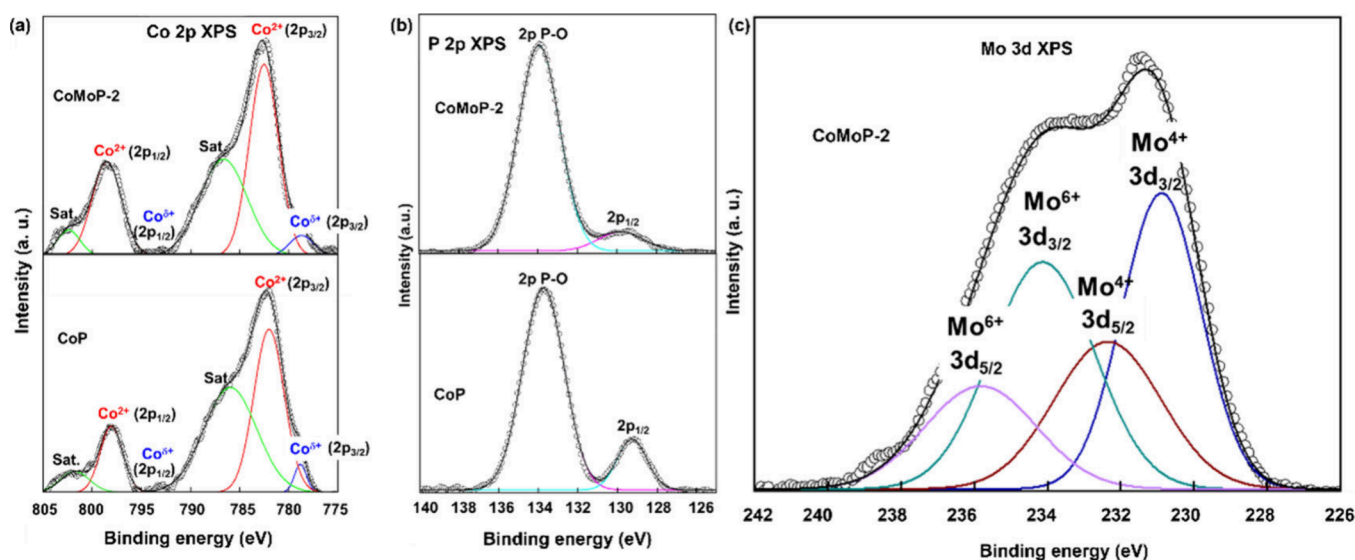

Figure 2. XPS spectra of the catalysts: (a) Co 2p, (b) P 2p, and (c) Mo 3d.

KOH solution at a pH of 13.9. The potential was converted to reversible hydrogen electrode according to the Nernst equation:[39]

$$E_{RHE} = E + 0.059 \times pH + 0.199 \qquad (1)$$

Additionally, the double-layer capacitance (C_{dl}) of each sample was calculated using cyclic voltammetry (CV) at various scan rates in a nonfaradic region. Additionally, the catalytic durability was analyzed using chronopotentiometry (CP) at 10 mA cm^{-2}. The catalyst preparation and loading were the same as described for the working electrodes. Additionally, durability was also studied using chronopotentiometry study at various current densities.

Determination of Turnover Frequency (TOF). Turnover frequency (TOF) was evaluated using the following equation:

$$Turn\ over\ frequency\ (TOF) = \frac{JA}{nFm} \qquad (2)$$

Here, J is the current density (A cm^{-2}), A is the geometric area of the electrode (cm^2), n is the number electron transfer number during the OER reaction (n = 4), F is the Faraday constant (96,485 C mol^{-1}), and m is the number of moles of active site loaded on the electrode. The obtained TOF is usually the minimum value, since partial exposure of active site is unavoidable.

RESULTS AND DISCUSSION

Structural and Morphological Properties. The surface morphology of the materials has been investigated using SEM as shown in Figure 1(a, b) and Figure S1(a−c). From the SEM results, it is evident that ZIF-67 has a rhombic dodecahedron morphology which is retained even after the phosphidation
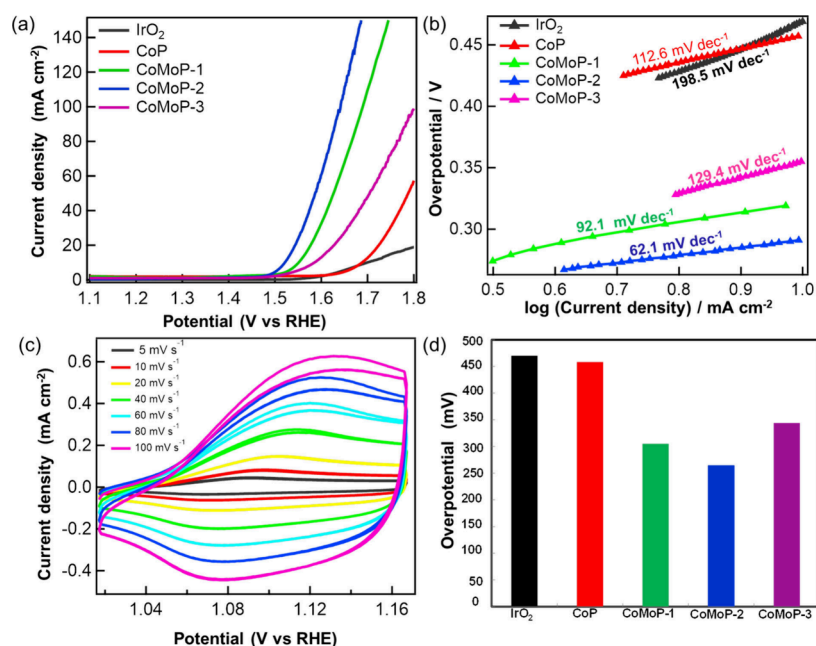
Figure 3. Electrocatalytic OER performance of the synthesized electrocatalyst. (a) Linear sweep voltammetry polarization curves of CoP, CoMoP-1, CoMoP-2, CoMoP-3, and IrO_2, (b) Tafel plot of all the catalysts, (c) CV curves conducted at various scan rates ranging from 5 to 100 mV s^{-1}, and (d) overpotential values of all the catalysts at 10 mA cm^{-2}.

process. Furthermore, the hollow rhombic dodecahedral morphology of the nanocages was also observed in the TEM image of CoP and CoMoP, which are depicted in Figure 1(c, d) and Figure S1(d, e). Additionally, porosity and textural characteristics of CoP and Mo-doped CoP were analyzed through BET surface analysis (Figure 1(f)). The nitrogen absorption isotherm gives rise to a surface area of 116.4 m^2 g^{-1} for CoMoP-2, which was much higher than that of CoP (34.07 m^2 g^{-1}). Based on the isotherms, Mo-doped CoP has higher surface area than that of undoped CoP. The incorporation of P and Mo was further confirmed by energy dispersive X-ray spectroscopy (EDS) measurement (Figures S2 and S3). The percentage of the doped Mo was 9.94 (wt %) for CoMoP-2 as observed through EDS analysis. The structure has been analyzed using powdered X-ray diffraction (PXRD) as depicted in Figure 1a and Figure S4. The XRD pattern of ZIF-67 is in good agreement with the literature, which confirms the pure phase of ZIF-67 (Figure S4(a)). After refluxing using sodium molybdate, the ZIF-67 phase disappears, and a new phase appears as shown in the PXRD pattern (Figure S4(b)). The PXRD pattern of CoMoNCs is consistent with the simulated pattern, as shown in Figure S4(b).

The characteristic peaks at 19, 33, 38, 52, and 58 correspond to the $Co(OH)_2$ phase (JCPDS 30-0443), and the peaks located at 19, 27, and 33 correspond to the phase of $CoMoO_4$ (JCPDS 21-0868). The formation of CoP and Mo-doped CoP (CoMoP-2) has been apparent in the respective PXRD patterns (Figure 1(e)), which give four distinct peaks that match well with the (011), (102), (202), and (301) planes of CoP which strongly matched with the standard JCPDS No. 29-0497.[36,37] From the XRD pattern, it is evident that the peak position of Mo-doped CoP is shifted to a lower 2Θ value, which signifies the widening of the interlayer distance. Additionally, different structural parameters were calculated from the XRD pattern using the methods described in the literature[40−44] and tabulated in Table S1. The crystalline size

of CoP was 8.34 nm, while after doping, the crystalline size of CoMoP-2 became 4.58 nm.

The chemical compositions of CoP and CoMoP-2 were confirmed using XPS, and the resulting data are depicted in Figures 2 and S5. From the XPS survey spectrum of both CoP and CoMoP-2, it is evident that Co, P, and O are present. These were further confirmed from the energy-dispersive X-ray spectroscopy (EDX) spectra of CoP as shown in Figures S2 and S3. From the XPS spectrum of Co 2p (Figure 2 (a)), the peaks located at 781.9 and 795.0 eV can be assigned to the presence of Co^{2+} $2p_{3/2}$ and Co^{2+} $2p_{1/2}$, respectively.[45,46] Additionally, the peaks located at 786.0 and 803.1 eV signify the existence of two apparent shakeup satellite peaks. Furthermore, a positive shift of the binding energy (BE) of Co 2p (778.8 eV) from that of metallic cobalt (777.9 eV) confirms that the cobalt in Co 2p contain partial positive charge (δ^+) with a small value ($0 < \delta < 2$).[47] On the other hand, the binding energy of P 2p (129.6 eV) shifted negatively to that of the elemental P (130.2 eV) so that the P has a partial negative charge (δ^-) in Co 2p. The direction of electron density transfer in Co 2p is from Co to P, as indicated by the changes in binding energies in the Co and P elements relative to their elementary substances, respectively.[48] Superficial oxidation of Co 2p generates a few oxidized P species in the sample. Therefore, the peaks at 133.2 eV in high BE range are assigned to the oxides.[49] Therefore, the presence of both Co_2P and Co phosphate are present in undoped CoP. Unlike $Co^{\delta+}$, no evidence of $Mo^{\delta+}$ (binding energy 228.6 eV) was observed. Rather, two valence states of Mo in the Mo 3d region spectrum was observed. The binding energy values of 230.5 and 232.5 eV are attributed to the Mo^{4+} state in the Mo $3d_{5/2}$ and Mo $3d_{3/2}$ regions, respectively. This state can be associated with molybdenum phosphate in the corresponding oxidation state.[50,51] The binding energies of 234.1 and 236.1 eV can be assigned to the Mo^{6+} state (molybdenum phosphate) in Mo $3d_{5/2}$ and Mo $3d_{3/2}$ regions, respectively.[52,53] The P 2p and Co 2p spectra are similar to those of undoped CoP. Therefore, it is

clear that although phosphates of both Co and Mo are present, the phosphide is present only in Co.
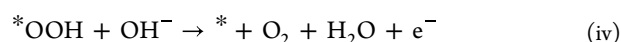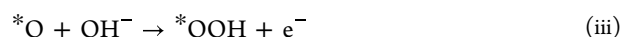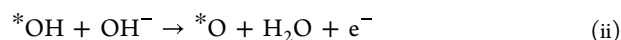
Additionally, we characterized the catalysts after the durability test to study the morphology and composition changes occurring during the catalytic activity. From Figure S6(b), it is evident that the morphology of the CoMoP-2 catalyst changes after the durability test. However, from PXRD and Raman spectroscopy (Figure S6(a) and S6(c)), it is evident that the structural feature of the catalyst changes. Especially, phases of cobalt oxide appeared due to the OER reaction.[34] Moreover, there is a shift in the peak position with a change in the peak intensity. Structural features were also evaluated using XPS, and it is evident that peak intensity and area are changed for both Co 2p and Mo 3d. From the Mo 3d XPS shown in Figure S7(b), it is evident that the peak intensity of Mo^{4+} species decreases but the intensity of Mo^{6+} increases; this may be due to the oxidation of Mo^{4+} to Mo^{6+}. In the case of Co 2p XPS spectra (Figure S7(a)), the peak intensity decreases; this is due to the dissolution of some cobalt ion during the catalytic reaction.

Catalytic Performance. The OER catalytic activity of CoMoP-2 catalysts was assessed in 1.0 M KOH by using three electrode systems. Additionally, CoP, CoMoP-1, and CoMoP-3 catalysts and commercial IrO_2 were also investigated for comparison. Figure 3a shows the LSV curves measured at a scan rate of 10 mV s^{-1}. The catalytic efficiency of CoP increases with the amount of Mo doping; however, very high Mo loading results in the decrease of catalytic activity. Additionally, the Tafel slope for IrO_2, CoP, CoMoP-3, CoMoP-1, and CoMoP-2 was 198.5, 112.6, 129.4, 92.1, and 62.1 mV dec^{-1}, respectively (Figure 3(b)). These values clearly indicate the favorable kinetics toward the OER catalytic activity.

Furthermore, the catalytic activity of a catalyst is strongly dependent on the electrochemically active surface area. To determine the electrochemical active sites of each catalyst, electrochemically active surface area (ECSA) was determined through C_{dl}, which was assessed from the CV curves measured at different scan rates ranges from 5 to 100 mV s^{-1} as shown in Figures 3c and S8(a−c). The C_{dl} value has a positive correlation with the ECSA. From Figure S9, it is evident that CoMoP-2 has a higher C_{dl} value than that of other catalysts, which confirms the highest ECSA among all. This higher ECSA value supports the higher OER activity of CoMoP-2. Furthermore, among these catalysts, CoMoP-2 shows the optimum catalytic activity with an onset potential of ∼1.49 V and an overpotential (at a current density of 10 mA cm^{-2}) of 264.4 mV (Figure 3(d)). On the contrary, other catalysts such as IrO_2, CoP, CoMoP-1, and CoMoP-3 give rise to overpotentials of 470.1, 458.1, 305.1, and 344.1 mV, respectively. Additionally electrochemical impedance spectroscopy (EIS) analysis was conducted to investigate the charge transfer resistance (R_{ct}) of CoP and CoMoP-2 catalysts in 1.0 M KOH solution, and the results obtained are shown in Figure S10. The Nyquist plots of EIS showed a semicircle for each of these catalysts, which implies the process that occurred was controlled by charge transfer. In EIS spectra, catalysts showing larger semicircles represent slower reaction kinetics in comparison to the catalysts showing smaller semicircles. This smaller semicircle of CoMoP-2 also supports higher catalytic activity of CoMoP-2 in comparison to CoP. The stability of the catalysts was tested using the CP method at the constant current density of 10 mA cm^{-2} for 4 h (Figure S11(a)). The

curves showed negligible decay of potential over this interval, which implies that this catalyst has considerable stability for application as a durable catalyst. The slight potential drop might be due to the consumption of OH$^-$ from electrolytes and the weakening of the active sites over the period.[25−28] Additionally, from Figure S11(b), it is evident that the LSV curve obtained after the 4 h stability test remained almost the same, which signifies its stability for a long period. Furthermore, durability was studied using a chronopotentiometry study at various current density studies, which is shown in Figure S12. Finally, the enhanced OER catalytic activity of CoMoP-2 can be attributed to its higher porosity and robust surface area generated with the introduction of molybdenum. Additionally, the catalytic activity increases with the amount of Mo-doping, suggesting that the unique structure, morphology and electronic interaction developed with the introduction of Mo results in the improvement of OER catalytic performance of the catalyst. Nevertheless, when Mo doping levels get too high, the buildup of materials worsens and causes many active sites to be inhibited, which lowers the materials' rate of utilization. Severe buildup also impedes charge transport, resulting in decreased electrochemical performance. In order to determine the intrinsic catalytic activity of the catalysts, the turnover frequency (TOF) of OER was determine at overpotential of 300 mV OER. CoP showed a TOF value of 0.013 s^{-1} in comparison to TOF value of 0.0278 s^{-1} for CoMoP-2. All of these data explain the reason for showing enhanced catalytic activity of CoMoP-2 in comparison to CoP.

The following four basic processes are involved in the generally acknowledged alkaline OER mechanisms:[54]

$$OH^- + * \rightarrow {}^*OH + e^- \tag{i}$$

$$^*OH + OH^- \rightarrow {}^*O + H_2O + e^- \tag{ii}$$

$$^*O + OH^- \rightarrow {}^*OOH + e^- \tag{iii}$$

$$^*OOH + OH^- \rightarrow * + O_2 + H_2O + e^- \tag{iv}$$

Here, * represents the active sites for OER. Since the medium is alkaline and plenty of OH$^-$ ions are present in the medium, water dissociation can be avoided in the first step and OH$^-$ ions can be used directly. The entire mechanism involves *OH, *O, and *OOH. The value of the Tafel slope (62.1 mV dec^{-1}) suggests that step (i) is very fast, and step (ii) (formation of *O) can be considered as the rate determining step. The Co active sites and lattice oxygen were found to be catalytically active toward OER as described by Grimaud et al. through in situ ^{18}O isotope labeling mass spectroscopy. The superior catalytic activity of the Mo-doped CoP than that of CoP may be due to the electron transport from the Mo to the adjacent Co species, which is followed by the transfer of electron to the H in HO* adsorption. The Mo-induced electron transfer toward the H would decrease the bond strength of H−O in the adsorbed HO species, facilitating the potential limiting deprotonation process and thereby boosting the OER catalytic performance.[55−57] Since the MOF-derived transition metal phosphide, sulphide, and nitride show instability under alkaline and acidic conditions, in situ Raman analysis during the catalytic activity study will explore the actual mechanism of the catalytic performance of these catalyst as reported in the literature.[58−60]

Table 1 compares the reported OER catalytic activity of MOF-derived CoP showing onset potential, overpotential, and

Table 1. Reported OER Performance for Some MOF Derived CoP Catalysts

Catalysts	Onset Potential (V)	Overpotential (10 mA cm^{-2})	Tafel slope (mV/dec)	ref.
Co phosphide/Co phosphate	–	310	65	29
CoP/NC	1.50	319	52	30
CoP nanorod	1.65	320	71	31
CoP-NS/C	1.50	292	64	32
CoP/rGO	–	340	70	33
CoP hollow polyhedron	1.65	400	57	34
Co/P/N-CNP-5	–	311	67.7	35
CoMoP-2	~1.49	264.4	62.1	This work

Tafel slope. Clearly, Mo-doped CoP showed an enhanced OER catalytic activity compared to some previously reported MOF-derived CoP, signifying the potential and possible practical applications of this catalyst.

CONCLUSIONS

We have fabricated a series of Mo-doped ZIF-67-derived CoP using a very facile dissolution−regrowth method. The Mo-doping results in the formation of hollow cobalt molybdenum nanocages (CoMoNCs). Phosphidation of these nanocages results in the formation of a stable and efficient OER catalyst. Study on the effect of the amount of Mo dopant suggests that Mo doping has a strong influence on the catalytic property of the as-synthesized catalyst. We observed an optimized doping condition for the OER catalytic activity. The optimized Mo-doped catalyst, CoMoP-2, exhibits efficient OER catalytic activity with an onset potential of ~1.49 V while showing an overpotential of 264.4 mV and a lower Tafel slope of 62.1 mV dec^{-1}. This enhanced catalytic activity is correlated with the higher porosity and surface area, which results in a higher electrochemical active surface area generated through the introduction of Mo. Finally, this study provides an efficient and facile strategy for the design of high-performance nonprecious OER electrocatalysts for application in electrochemical energy conversion devices.

ASSOCIATED CONTENT

Ⓢ Supporting Information

The Supporting Information is available free of charge at https://pubs.acs.org/doi/10.1021/acsomega.4c00403.

> SEM and TEM images of ZIF-67, CoMoP-1, and CoMoP-3; EDX analysis of prepared samples; PXRD pattern of prepared catalysts; XPS survey spectra; CV curves of prepared catalysts, current density vs scan rate, calculated C_{dl} values and ECSA values of catalysts; Nyquist plots of CoP and CoMoP-2; catalysts stability test of CoMoP-2 (PDF)

AUTHOR INFORMATION

Corresponding Author

Shinya Hayami − *Institute of Industrial Nanomaterials (IINa), Kumamoto University, Chuo-ku, Kumamoto 860-8555, Japan; International Research Center for Agricultural and Environmental Biology (IRCAEB), Chuo-ku, Kumamoto 860-8555, Japan;* ⓞ orcid.org/0000-0001-8392-2382; Email: hayami@kumamoto-u.ac.jp

Authors

Mohammad Atiqur Rahman − *Department of Chemistry, Graduate School of Science and Technology, Kumamoto University, Chuo-ku, Kumamoto 860-8555, Japan; Department of Chemistry, Comilla University, Cumilla 3500, Bangladesh; International Research Organization for Advanced Science and Technology, Kumamoto University, Chuo-ku, Kumamoto 860-8555, Japan*

Ze Cai − *Department of Chemistry, Graduate School of Science and Technology, Kumamoto University, Chuo-ku, Kumamoto 860-8555, Japan*

Zannatul Mumtarin Moushumy − *Department of Applied Chemistry and Biochemistry, Graduate School of Science and Technology, Kumamoto University, Chuo-ku, Kumamoto 860-8555, Japan*

Ryuta Tagawa − *Department of Chemistry, Graduate School of Science and Technology, Kumamoto University, Chuo-ku, Kumamoto 860-8555, Japan*

Yoshiharu Hidaka − *Department of Chemistry, Graduate School of Science and Technology, Kumamoto University, Chuo-ku, Kumamoto 860-8555, Japan*

Chiyu Nakano − *Research Core for Interdisciplinary Sciences, Okayama University, Kita-ku, Okayama 700-8530, Japan*

Md. Saidul Islam − *Department of Chemistry, Graduate School of Science and Technology, Kumamoto University, Chuo-ku, Kumamoto 860-8555, Japan; Institute of Industrial Nanomaterials (IINa), Kumamoto University, Chuo-ku, Kumamoto 860-8555, Japan;* ⓞ orcid.org/0000-0003-2857-7891

Yoshihiro Sekine − *Department of Chemistry, Graduate School of Science and Technology, Kumamoto University, Chuo-ku, Kumamoto 860-8555, Japan; Priority Organization for Innovation and Excellence, Kumamoto University, Chuo-ku, Kumamoto 860-8555, Japan;* ⓞ orcid.org/0000-0001-9513-392X

Yuta Nishina − *Research Core for Interdisciplinary Sciences, Okayama University, Kita-ku, Okayama 700-8530, Japan;* ⓞ orcid.org/0000-0002-4958-1753

Shintaro Ida − *Institute of Industrial Nanomaterials (IINa), Kumamoto University, Chuo-ku, Kumamoto 860-8555, Japan;* ⓞ orcid.org/0000-0002-0032-1897

Complete contact information is available at:
https://pubs.acs.org/10.1021/acsomega.4c00403

Author Contributions

The manuscript was prepared through effort from all authors. Each author has given permission to the final version of the manuscript.

Notes

The authors declare no competing financial interest.

ACKNOWLEDGMENTS

REFERENCES

(1) Li, Q.; Guo, H.; Xue, R.; Wang, M.; Xu, M.; Yang, W.; Zhang, J.; Yang, W. Self-assembled Mo doped Ni-MOF nanosheets based electrode material for high performance battery-supercapacitor hybrid device. *Int. J. Hydrogen Energy* **2020**, *45* (41), 20820.

(2) Zhao, Q.; Yan, Z.; Chen, C.; Chen, J. Spinels: Controlled Preparation, Oxygen reduction/Evolution Reaction Application and Beyond. *Chem. Rev.* **2017**, *117*, 10121.

(3) Siracusano, S.; Van Dijk, N.; Payne-Johnson, E.; Baglio, V.; Aricò, A. S. Nanosized IrO_x and $IrRuO_x$ electrocatalysts for the O_2 evolution reaction in PEM water electrolysers. *Appl. Catal. B: Envir.* **2015**, *164*, 488−495.

(4) Gasteiger, H. A.; Kocha, S. S.; Sompalli, B.; Wagner, F. T. Activity benchmarks and requirements for Pt, Pt-alloy, and non-Pt oxygen reduction catalysts for PEMFCs. *Appl. Catal. B: Envir.* **2005**, *56*, 9.

(5) Shudo, Y.; Fukuda, M.; Islam, M. S.; Kuroiwa, K.; Sekine, Y.; Karim, M. R.; Hayami, S. 3D Porous Ni/NiO_x as a bifunctional oxygen electrocatalyst derived from Freeze-dried $Ni(OH)_2$. *Nanoscale.* **2021**, *13*, 5530.

(6) Tsutsumi, M.; Islam, M. S.; Karim, M. R.; Rabin, N. N.; Ohtani, R.; Nakamura, M.; Lindoy, L. F.; Hayami, S. Tri-functional OER, HER and ORR Electrocatalyst Electrodes from In Situ Metal-Nitrogen Co-doped Oxidized Graphite Rods. *Bull. Chem. Soc. Jpn.* **2017**, *90*, 950−954.

(7) Banerjee, R.; Phan, A.; Wang, B.; Knobler, C.; Furukawa, H.; O'Keeffe, M.; Yaghi, O. M. High-Throughput Synthesis of Zeolitic Imidazolate Frameworks and Application to CO_2 Capture. *Science* **2008**, *319*, 939.

(8) Rieter, W. J.; Taylor, K. M. L.; Lin, W. Surface Modification and Functionalization of Nanoscale Metal-Organic Frameworks for Controlled Release and Luminescence Sensing. *J. Am. Chem. Soc.* **2007**, *129*, 9852.

(9) Palaniselvam, T.; Biswal, B. P.; Banerjee, R.; Kurungot, S. Zeolitic Imidazolate Framework (ZIF)-Derived, Hollow-Core, Nitrogen-Doped Carbon Nanostructures for Oxygen-Reduction Reactions in PEFCs. *Chem.—Eur. J.* **2013**, *19*, 9335.

(10) Liu, X.; Dong, J.; You, B.; Sun, Y. Competent overall water-splitting electrocatalysts derived from ZIF-67 grown on carbon cloth. *RSC Adv.* **2016**, *6*, 73336.

(11) Chaikittisilp, W.; Torad, N. L.; Li, C.; Imura, M.; Suzuki, N.; Ishihara, S.; Ariga, K.; Yamauchi, Y. Synthesis of Nanoporous Carbon−Cobalt-Oxide Hybrid Electrocatalysts by Thermal Conversion of Metal−Organic Frameworks. *Chem.- Eur. J.* **2014**, *20*, 4217−4221.

(12) Dou, S.; Li, X.; Tao, L.; Huo, J.; Wang, S. Cobalt nanoparticle-embedded carbon nanotube/porous carbon hybrid derived from MOF-encapsulated Co_3O_4 for oxygen electrocatalysis. *Chem. Commun.* **2016**, *52*, 9727−9730.

(13) Wang, H.; Zhang, L.; Zhang, W.; Sun, S.; Yao, S. Highly Efficient Spatial Three-Level CoP@ZIF-8/pNF Based on Modified Porous NF as Dual Functional Electrocatalyst for Water Splitting. *Nanomaterials* **2023**, *13* (8), 1386.

(14) Gong, C.; Li, W.; Lei, Y.; He, X.; Chen, H.; Du, X.; Fang, W.; Wang, D.; Zhao, L. Interfacial engineering of ZIF-67 derived CoSe/$Co(OH)_2$ catalysts for efficient overall water splitting. *Composite Part B: Engineering* **2022**, *236*, 109823.

(15) Li, X.; Jiang, Q.; Dou, S.; Deng, L.; Huo, J.; Wang, S. ZIF-67-derived Co-NC@CoP-NC nanopolyhedra as an efficient bifunctional oxygen electrocatalyst. *J. Mater. Chem. A* **2016**, *4*, 15836.

(16) Howarth, A. J.; Liu, Y.; Li, P.; Li, Z.; Wang, T. C.; Hupp, J. T.; Farha, O. K. Chemical, thermal and mechanical stabilities of metal−organic frameworks. *Nat. Rev. Mater.* **2016**, *1*, 15018.

(17) Lu, X.-F.; Liao, P.-Q.; Wang, J.-W.; Wu, J.-X.; Chen, X.-W.; He, C.-T.; Zhang, J.-P.; Li, G.-R.; Chen, X.-M. An alkaline-stable, metal hydroxide mimicking metal−organic framework for efficient electrocatalytic oxygen evolution. *J. Am. Chem. Soc.* **2016**, *138*, 8336.

(18) Pan, Y.; Sun, K.; Liu, S.; Cao, X.; Wu, K.; Cheong, W.-C.; Chen, Z.; Wang, Y.; Li, Y.; Liu, Y.; Wang, D.; Peng, Q.; Chen, C.; Li, Y. Core−Shell ZIF-8@ZIF-67-Derived CoP Nanoparticle-Embedded N-Doped Carbon Nanotube Hollow Polyhedron for Efficient Overall Water Splitting. *J. Am. Chem. Soc.* **2018**, *140* (7), 2610.

(19) Tong, X.; Liao, W.; Fu, Y.; Qian, M.; Dai, H.; Mei, L.; Zhai, Y.; Chen, T.; Yang, L.; Yang, Q. Ag-doped CoP Hollow Nanoboxes as Efficient Water Splitting Electrocatalysts and Antibacterial Materials. *ChemistrySelect* **2022**, *7*, No. e202202343.

(20) Prieto, G.; Tüysüz, H.; Duyckaerts, N.; Knossalla, J.; Wang, G. H.; Schüth, F. Hollow Nano-and Microstructures as Catalysts, *Chem. Rev.* **2016**, *116*, 14056.

(21) Zhang, L.; Zhu, Y.-X.; Hu, G.-Z. 11-MOFs-derived hollow structure as a versatile platform for highly-efficient multifunctional electrocatalyst toward overall water-splitting and Zn-air battery. *Nanomaterials* **2022**, *1*, 251.

(22) Wang, X.; Feng, J.; Bai, Y. C.; Zhang, Q.; Yin, Y. D. Synthesis, Properties, and Applications of Hollow Micro-/Nanostructures. *Chem. Rev.* **2016**, *116*, 10983.

(23) Xia, W.; Zhu, J.; Guo, W.; An, L.; Xia, D.; Zou, R. Well-defined carbon polyhedrons prepared from nano metal−organic frameworks for oxygen reduction. *J. Mater. Chem. A* **2014**, *2*, 11606.

(24) Lyu, F.; Bai, Y.; Li, Z.; Xu, W.; Wang, Q.; Mao, J.; Wang, L.; Zhang, X.; Yin, Y. Self-templated fabrication of $CoO-MoO_2$ nanocages for enhanced oxygen evolution. *Adv. Funct. Mater.* **2017**, *27*, 1702324.

(25) Huang, C.; Hao, C.; Ye, Z.; Zhou, S.; Wang, X.; Zhu, L.; Wu, J. In situ growth of ZIF-8-derived ternary $ZnO/ZnCo_2O_4/NiO$ for high performance asymmetric supercapacitors. *Nanoscale* **2019**, *11*, 10114.

(26) Yin, Z.; Liu, X.; Cui, M.; Cao, Z.; Liu, A.; Gao, L.; Ma, T.; Chen, S.; Li, Y. Template synthesis of molybdenum-doped NiFe-layered double hydroxide nanotube as high efficiency electrocatalyst for oxygen evolution reaction. *Materials Today Sustainability* **2022**, *17*, 100101.

(27) Dang, Y.; Han, P.; Li, Y.; Zhang, Y.; Zhou, Y. Low-crystalline mixed Fe-Co-MOFs for efficient oxygen evolution electrocatalysis. *J. Mater. Sci.* **2020**, *55*, 13951.

(28) Yu, C.; Lu, J. J.; Luo, L.; Xu, F.; Shen, P. K.; Tsiakaras, P.; Yin, S. B. Bifunctional catalysts for overall water splitting: CoNi oxyhydroxide nanosheets electrodeposited on titanium sheets. *Electrochim. Acta* **2019**, *301*, 449.

(29) Yang, Y.; Fei, H.; Ruan, G.; Tour, J. M. Porous Cobalt-Based Thin Film as a Bifunctional Catalyst for Hydrogen Generation and Oxygen Generation. *Adv. Mater.* **2015**, *27*, 3175−3180.

(30) You, B.; Jiang, N.; Sheng, M.; Gul, S.; Yano, J.; Sun, Y. High-Performance Overall Water Splitting Electrocatalysts Derived from Cobalt-Based Metal−Organic Frameworks. *Chem. Mater.* **2015**, *27* (22), 7636−7642.

(31) Chang, J.; Xiao, Y.; Xiao, M.; Ge, J.; Liu, C.; Xing, W. Surface Oxidized Cobalt-Phosphide Nanorods As an Advanced Oxygen Evolution Catalyst in Alkaline Solution. *ACS Catal.* **2015**, *5* (11), 6874−6878.

(32) Li, H.; Ke, F.; Zhu, J. MOF-Derived Ultrathin Cobalt Phosphide Nanosheets as Efficient Bifunctional Hydrogen Evolution Reaction and Oxygen Evolution Reaction Electrocatalysts. *Nanomaterials* **2018**, *8*, 89.

(33) Jiao, L.; Zhou, Y.-X.; Jiang, H.-L. Metal−organic framework-based CoP/reduced graphene oxide: high-performance bifunctional electrocatalyst for overall water splitting. *Chem. Sci.* **2016**, *7*, 1690−1695.

(34) Liu, M.; Li, J. Cobalt Phosphide Hollow Polyhedron as Efficient Bifunctional Electrocatalysts for the Evolution Reaction of Hydrogen and Oxygen. *Acs Appl. Mater. Inter.* **2016**, *8*, 2158−2165.

(35) Tang, F.; Gao, Z.; Jin. Pre-leaching strategy for tuning porosity and composition to generate $Co_2P/Co@P/N$-doped carbon towards highly efficient bifunctional oxygen electrocatalysis. *Electrochim. Acta* **2020**, *337*, 135807.

(36) Zhu, K. J.; Liu, G.; Wang, Y. J.; Liu, J.; Li, S. T.; Yang, L. Y.; Liu, S. L.; Wang, H.; Xie, T. Metal-Organic Frameworks derived novel hierarchical durian-like nickel sulfide (NiS2) as an anode material for high-performance sodium-ion batteries. *Mater. Lett.* **2017**, *197*, 180−183.

(37) Wu, W.; Wu, X.-Y.; Wang, S.-S.; Lu, C.-Z. Highly efficient hydrogen evolution from water electrolysis using nanocrystalline transition metal phosphide catalysts. *RSC Adv.* **2018**, *8*, 39291−39295.

(38) Afkhami-Ardekani, M.; Naimi-Jamal, M. R.; Doaee, S.; Rostamnia, S. Solvent-Free Mechanochemical Preparation of Metal-

Organic Framework ZIF-67 Impregnated by Pt Nanoparticles for Water Purification. *Catalysts* **2023**, *13*, 9.

(39) Wakamatsu, S.; Islam, M. S.; Shudo, Y.; Fukuda, M.; Tagawa, R.; Goto, N.; Koinuma, M.; Sekine, Y.; Hayami, S. An efficient oxygen evolution reaction catalyst using Ni−Co layered double hydroxide anchored on reduced graphene oxide. *Energy Adv.* **2023**, *2*, 1375−1380.

(40) Munawar, T.; Bashir, A.; Nadeem, M. S.; Mukhtar, F.; Manzoor, S.; Ashiq, M. N.; Khan, S. A.; Koc, M.; Iqbal, F. Electrochemical Performance Evaluation of Bimetallic Sulfide Nanocomposite with Fullerene (CeNdS/C60) for Efficient Oxygen Evolution Reaction (OER). *Energy Fuels* **2023**, *37*, 1370−1386.

(41) Bashir, A.; Munawar, T.; Mukhtar, F.; Nadeem, M. S.; Manzoor, S.; Ashiq, M. N.; Khan, S. A.; Koc, M.; Iqbal, F. Dual-functional fullerene supported NiO-based nanocomposite: Efficient electrocatalyst for OER and photocatalyst for MB dye degradation. *Mater. Chem. Phys.* **2023**, *293*, 126886.

(42) Nadeem, M. S.; Munawar, T.; Mukhtar, F.; Naveed ur Rahman, M.; Riaz, M.; Iqbal, F. Enhancement in the photocatalytic and antimicrobial properties of ZnO nanoparticles by structural variations and energy bandgap tuning through Fe and Co co-doping. *Ceram. Int.* **2021**, *47*, 11109−11112.

(43) Munawar, T.; Bashir, A.; Nadeem, M. S.; Mukhtar, F.; Manzoor, S.; Ashiq, M. N.; Khan, S. A.; Koc, M.; Iqbal, F. Core-shell CeO2@C60 hybrid serves as a dual-functional catalyst: Photocatalyst for organic pollutant degradation and electrocatalyst for oxygen evolution reaction. *Ceram. Int.* **2023**, *49*, 8447−8462.

(44) Nadeem, M. S.; Munawar, T.; Mukhtar, F.; Naveed ur Rahman, M.; Riaz, M.; Hussain, A.; Iqbal, F. Hydrothermally derived co, Ni co-doped ZnO nanorods; structural, optical, and morphological study. *Opt. Mater.* **2021**, *111*, 110606.

(45) Liu, D. N.; Chen, T.; Zhu, W.; Cui, L.; Asiri, A. M.; Lu, Q.; Sun, X. P. Cobalt phosphide nanowires: an efficient electrocatalyst for enzymeless hydrogen peroxide detection. *Nanotechnology* **2016**, *27*, 1−6.

(46) Liang, F.; Huang, L.; Tian, L.; Li, J. Y.; Zhang, H. J.; Zhang, S. W. Microwaveassisted hydrothermal synthesis of cobalt phosphide nanostructures for advanced supercapacitor electrodes. *CrystEngComm* **2018**, *20*, 2413−2420.

(47) Huang, Z. P.; Chen, Z. Z.; Chen, Z. B.; Lv, C. C.; Humphrey, M. G.; Zhang, C. Cobalt phosphide nanorods as an efficient electrocatalyst for the hydrogen evolution reaction. *Nano Energy* **2014**, *9*, 373−382.

(48) Burns, A. W.; Layman, K. A.; Bale, D. H.; Bussell, M. E. Understanding the relationship between composition and hydrodesulfurization properties for cobalt phosphide catalysts. *ApplCatal. A Gen* **2008**, *343*, 68−76.

(49) Liu, Y. W.; Cao, X. Q.; Kong, R. M.; Du, G.; Asiri, A. M.; Lu, Q.; Sun, X. P. Cobalt phosphide nanowire array as an effective electrocatalyst for non-enzymatic glucose sensing. *J. Mater. Chem. B* **2017**, *5*, 1901−1904.

(50) Adam, A.; Suliman, M. H.; Dafalla, H.; Al-Arfaj, A. R.; Siddiqui, M. N.; Qamar, M. Rationally Dispersed Molybdenum Phosphide on Carbon Nanotubes for the Hydrogen Evolution Reaction. *ACS Sustainable Chem. Eng.* **2018**, *6*, 11414−11423.

(51) Jiang, Y.; Shen, Y.; Dong, J.; Tan, S.; Wei, Q.; Xiong, F.; Li, Q.; Liao, X.; Liu, Z.; An, Q.; Mai, L. Surface Pseudocapacitive Mechanism of Molybdenum Phosphide for High-Energy and High-Power Sodium-Ion Capacitors. *Adv. Energy Mater.* **2019**, *9*, 1900967.

(52) Yang, J.; Zhang, F.; Wang, X.; He, D.; Wu, G.; Yang, Q.; Hong, X.; Wu, Y.; Li, Y. Porous Molybdenum Phosphide Nano-Octahedrons Derived from Confined phosphorization in UIO-66 for Efficient Hydrogen Evolution. *Angew. Chem., Int. Ed.* **2016**, *55*, 12854−12858.

(53) Watson, I. M.; Connor, J. A.; Whyman, R. Non-crystalline chromium, molybdenum and tungsten phosphate films prepared by metal organic chemical vapour deposition. *Thin Solid Films* **1991**, *201*, 337−349.

(54) Zhang, S.; Wei, N.; Yao, Z.; Zhao, X.; Du, M.; Zhou, Q. Oxygen vacancy-based ultrathin Co3O4 nanosheets as a highefficiency electrocatalyst for oxygen evolution reaction. *Int. J. Hydrogen Energy* **2021**, *46*, 5286.

(55) Grimaud, A.; Diaz-Morales, O.; Han, B.; Hong, W. T.; Lee, Y. L.; Giordano, L.; Stoerzinger, K. A.; Koper, M. T. M.; Shao-Horn, Y. Activating lattice oxygen redox reactions in metal oxides to catalyse oxygen evolution. *Nat. Chem.* **2017**, *9*, 457.

(56) Zhu, Y.; Tahini, H. A.; Hu, Z.; Yin, Y.; Lin, Q.; Sun, H.; Zhong, Y.; Chen, Y.; Zhang, F.; Lin, H. J.; Chen, C. T.; Zhou, W.; Zhang, X.; Smith, S. C.; Shao, Z.; Wang, H. Boosting oxygen evolution reaction by activation of lattice-oxygen sites in layered Ruddlesden-Popper oxide. *EcoMat* **2020**, *2*, No. e12021.

(57) Wang, X.; Pan, Z.; Chu, X.; Huang, K.; Cong, Y.; Cao, R.; Sarangi, R.; Li, L.; Li, G.; Feng, S. Atomic-scale insights into surface lattice oxygen activation at the spinel/perovskite interface of Co3O4/La0.3Sr0.7CoO3. *Angew. Chem. Int.* **2019**, *58*, 11720.

(58) Golubeva, M. A.; Mukhtarova, M.; Sadovnikov, A. A.; Maximov, A. L. Bulk Molybdenum and Tungsten Phosphides for Selective Phenol Production from Guaiacol. *ACS Omega* **2022**, *7*, 40586−40595.

(59) Zhou, J.; Huang, C.; Zhou, Q.; Xie, Y.; Yang, L.; Yu, L.; Yu, Y. Electronic Structure Regulation of Nickel Phosphide for Efficient Overall Water Splitting, Inorg. *Chem.* **2022**, *61* (24), 9318−9327.

(60) Zhou, J.; Yu, L.; Zhou, Q.; Huang, C.; Zhang, Y.; Yu, B.; Yu, Y. Ultrafast fabrication of porous transition metal foams for efficient electrocatalytic water splitting. *Appl. Catal. B: Environ.* **2021**, *288*, 120002.